

Daedalus: Breaking Non-Maximum Suppression in Object Detection via Adversarial Examples

Derui Wang^{1,2}, Chaoran Li¹, Sheng Wen¹, Surya Nepal², Yang Xiang¹

¹Swinburne University of Technology, Australia

²CSIRO's Data61, Australia

{deruiwang, chaoranli, swen, yxiang}@swin.edu.au, surya.nepal@data61.csiro.au

Abstract—We demonstrated that Non-Maximum Suppression (NMS), which is commonly used in object detection tasks to filter redundant detection results, is no longer secure. NMS has always been an integral part of object detection algorithms. Currently, Fully Convolutional Network (FCN) is widely used as the backbone architecture of object detection models. Given an input instance, since FCN generates end-to-end detection results in a single stage, it outputs a large number of raw detection boxes. These bounding boxes are then filtered by NMS to make the final detection results.

In this paper, we propose an adversarial example attack which triggers malfunctioning of NMS in the end-to-end object detection models. Our attack, namely Daedalus, manipulates the detection box regression values to compress the dimensions of detection boxes. Henceforth, NMS will no longer be able to filter redundant detection boxes correctly. And as a result, the final detection output contains extremely dense false positives. This can be fatal for many object detection applications such as autonomous vehicle and smart manufacturing industry. Our attack can be applied to different end-to-end object detection models. Furthermore, we suggest crafting robust adversarial examples by using an ensemble of popular detection models as the substitutes. Considering that model reusing is commonly seen in real-world object detection scenarios, Daedalus examples crafted based on an ensemble of substitutes can launch attacks without knowing the details of the victim models. Our experiments demonstrate that our attack effectively stops NMS from filtering redundant bounding boxes. As the evaluation results suggest, Daedalus increases the false positive rate in detection results to 99.9% and reduces the mean average precision scores to 0, while maintaining a low cost of distortion on the original inputs and keeping the perturbation on the adversarial examples imperceptible.

Index Terms—Deep neural network, adversarial example, object detection, cyber security

I. INTRODUCTION

Object detection is a fundamental operation in the field of computer vision and is repeatedly used in the areas of autonomous vehicles, robotics, surveillance system, and biometric authentications. Convolutional Neural Network (CNN) is embedded in the core of many state-of-the-art object detection models. These models can be classified into two broad categories: single-stage detection models (e.g. SSD [31], RetinaNet [28], You-Only-Look-Once (YOLO) [46], YOLO-9000 [47], and YOLO-v3 [48]) and two-stage detection models (e.g. Fast R-CNN [13], Faster R-CNN [49]). Single-stage ones have become successful since they perform end-to-end detection which has low computational overhead and is competitively

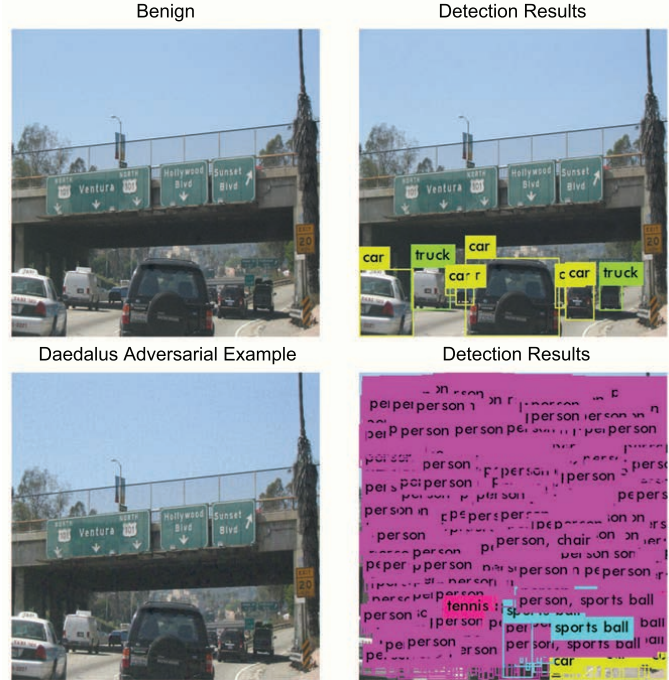


Fig. 1. A demo of the Daedalus attack on YOLO-v3. The image on the left side of the first row is an original image taken from the COCO dataset [29]. The object detection results on the image are given on the right side. An adversarial example and the object detection results of the adversarial example are shown in the second row. It can be observed that the adversarial example significantly increases the number of final detection boxes after NMS. In other words, the detector becomes non-viable since the final detection is noisy. Meanwhile, the perturbation on the adversarial example remains imperceptible.

accurate. Current end-to-end detection models are built upon Fully Convolutional Network (FCN) backbones. However, FCNs output a large number of redundant detection results that shall be filtered before the final results are produced.

To filter the redundant detection boxes, Non-Maximum Suppression (NMS) is performed as a key step in the object detection procedure [41]. NMS has been an integral component in many object detection algorithms for around 50 years. It relies on non-differentiable, hard-coded rules to discard redundant boxes. It is used in both single-stage and two-stage detection algorithms. Beyond object detection, NMS is also being used in face recognition, face verification and keypoint detection [50]. NMS has also inspired refinement

algorithms in two-stage detection models [6]. Some recent works tried to use a differentiable model to learn NMS [20]–[22], [45]. Another work suggested using soft-NMS to improve the filtering performance [3]. Once the NMS component in an object detection system does not work properly, the system can no longer give out correct detection results.

CNN is known to be vulnerable to adversarial example attacks [1]. To a human eye, an adversarial image can be indistinguishable from the original one, but it can cause misclassification in a CNN based classifier. Nevertheless, due to the difference between object detection and image classification, attacks on classifiers cannot be directly launched on object detection models. Recently, an adversarial example has been crafted for the object detection and segmentation task [57]. This attack follows the same principles as the ones that craft adversarial examples for classifiers. Such attacks on detection models, result in the misclassification of the detected objects. Therefore, in this paper, we refer to this type of example as misclassification adversarial example. However, the exploitable vulnerability of CNN based object detection models is more than just the misclassification of detected objects.

In this paper, we propose a novel adversarial example attack for NMS, which can be universally applied to any other end-to-end differentiable object detection model. A demonstration of our attack is shown in Fig.1. As it can be seen, a properly crafted adversarial example can trigger malfunctioning of the NMS component in YOLO-v3, in a way that it outputs dense and noisy detection results. We named this attack Daedalus since it creates a maze composed of false positive detection results. This attack can be fatal in the application scenarios such as autonomous vehicle or manufacturing industrial process. Theoretically, our attack can be applied to the feature maps of various detectors to generate adversarial examples. In our experiments, we exploited the latest version of YOLO (i.e. YOLO-v3) as our substitute to craft the adversarial examples. Compared to other state-of-the-art object detection models, YOLO-v3 runs significantly faster and can achieve a comparable detection performance [48]. Furthermore, it is easy to obtain a well-trained YOLO-v3 model as a substitute since it is open-source. To demonstrate the generality of our attack, we also used the same approach to attack another popular model (i.e. RetinaNet [28]), which was completely different in backbone and feature map. Moreover, we suggest using **ensemble of substitutes** (i.e., ensemble of popular detection models as the substitutes) in Daedalus attack to break black-box detection models. Model reusing is common in real-world object detection tasks [30]. Therefore, an attacker can launch black-box attacks on popular object detection models leveraging universal adversarial examples which work effectively against all the possible models. As suggested by our experiments, robust Daedalus examples generated by using an ensemble of popular backbone networks as the substitutes can launch the attack in a black-box scenario. We summaries our contributions as follows:

- We analyse a vulnerability of NMS;

- We propose a novel adversarial example attack which aims at breaking NMS (unlike the existing state-of-the art attacks that merely target misclassification);
- We propose new adversarial loss functions to generate NMS adversarial examples;
- The proposed ensemble-of-substitutes attack can generate robust adversarial examples that can make NMS malfunction in multiple models, simultaneously;
- We systematically evaluate our attack and based on the results, show that it is effective against the state-of-the-art object detection models.

The paper is organised as follows: Section II introduces the background of adversarial example crafting methods, YOLO-v3, and NMS. Section III describes the design of Daedalus attack. Section IV compares and selects loss functions from the candidates, and systematically evaluates the performance of our attack. Section V discusses the possibility of applying Daedalus adversarial examples on soft-NMS, RetinaNet, and black-box models. We also post the dilemma of defending against Daedalus attack in this section. Section VI reviews the related work relevant to our study. Section VII draws a conclusion on the paper and presents our future work.

II. PRIMER

A. Adversarial example

Suppose a deep neural network model is equal to a non-convex function F . In general, given an image x along with the rightful one-hot encoded label y_{true} , an attacker searches for the adversarial example x_{adv} . We first review some of the state-of-the-art adversarial example crafting methods for image classification in this section.

FGSM. Fast Gradient Sign Method (FGSM) is able to generate adversarial examples rapidly [14]. FGSM perturbs an image in the image space towards gradient sign directions. FGSM can be described using the following formula:

$$x_{adv} \leftarrow x + \epsilon sgn(\nabla_x L(F(x), y_{true})), \quad (1)$$

where L is the loss function (a cross-entropy function is typically used to compute the loss). $F(x)$ is the softmax layer output from the model F . ϵ is a hyper-parameter which controls the amount of distortion on the crafted image, and sgn is the sign function. FGSM requires gradients to be computed only once. Thus, FGSM can craft large batches of adversarial examples in a very short period.

IGS. Iterative Gradient Gign (IGS) attack perturbs pixels in each iteration instead of a one-off perturbation [26]. In each round, IGS perturbs the pixels towards the gradient sign direction and clips the perturbation using a small value ϵ . The adversarial example in the i -th iteration is stated as follows:

$$x_{adv}^i = x_{adv}^{i-1} - clip_\epsilon(\alpha \cdot sgn(\nabla_x L(F(x_{adv}^{i-1}), y_{true}))) \quad (2)$$

Compared to FGSM, IGS can produce adversarial examples with higher misclassification confidence.

JSMA. Jacobian-based Saliency Map Attack (JSMA) iteratively perturbs important pixels defined by the Jacobian matrix based on the model output and input features [42]. The method first calculates the forward derivatives of the neural network output with respect to the input example. Based on the adversarial saliency map that demonstrates the most influential pixels which should be perturbed, an attacker can perturb a few important pixels in each iteration, until the example image becomes adversarial. Based on two versions of the saliency map, an attacker can increase the value of the influential pixels in each iteration to perform targeted adversarial examples, or decrease pixel values to get non-targeted examples.

Deepfool. Deepfool generates an adversarial example with a minimum distortion on the original image [40]. The basic idea is to search for the closest decision boundary and then perturb x towards the decision boundary. Deepfool iteratively perturbs x until x is misclassified. The modification on the image in each iteration for a binary classifier is achieved as follows:

$$r_i \leftarrow -\frac{F(x)}{\|\nabla F(x)\|_2^2} \nabla F(x) \quad (3)$$

Deepfool employs the linearity assumption of the neural network to simplify the optimisation process. We use the L_∞ version of Deepfool in our evaluation.

Carlini&Wagner L_2 . This method is reportedly able to make defensive distillation invalid [5]. This study has explored crafting adversarial examples under three distance metrics (i.e. L_0 , L_2 , and L_∞) and seven modified objective functions. We use Carlini&Wagner L_2 , which is based on the L_2 metric, in our experiment. The method first redesigns the optimisation objective $f(x_{adv})$ as follows:

$$f(x_{adv}) = \max(\max\{Z(x_{adv})_i : i \neq l\} - Z(x_{adv})_l, -\kappa) \quad (4)$$

where $Z(x_{adv})$ are the output logits of the neural network, and κ is a hyper-parameter for adjusting adversarial example confidence at the cost of enlarging the distortion on the adversarial image. Then, it adapts Limited-memory BroydenFletcherGoldfarbShanno algorithm (L-BFGS) to solve the box-constraint problem:

$$\begin{aligned} \min_{\delta} & \|\delta\|_2 + c \cdot f(x + \delta) \\ \text{s.t. } & x + \delta \in [0, 1]^n, \end{aligned} \quad (5)$$

wherein $x + \delta = x_{adv}$. The optimization variable is changed to $\omega : \delta = \frac{1}{2}\tanh(\omega) + 1 - x$. According to the results, this method has achieved 100% attacking success rate on the distilled networks in a white-box setting. By changing the confidence, this method can also have targeted transferable examples to perform a black-box attack.

B. YOLO-v3

You Only Look Once (YOLO) is an FCN based object detection model [46]. YOLO has achieved the state-of-the-art performance on standard detection tasks such as PASCAL

VOC [11] and COCO [29]. Since it is built on the end-to-end architecture, YOLO is able to perform object detection in real-time. Over the past years, YOLO has been updated to YOLO-v2/YOLO-9000 [47], and the current YOLO-v3 [48]. YOLO has been applied in video object detection [51] and robotics [34]. YOLO is commonly studied in the research of road sign detection and recognition for autonomous car [59]. Moreover, since YOLO is open-source, it can be deployed in mobile phone applications or other commercial applications.

The backbone of YOLO-v3 is a 53-layer FCN (i.e. Darknet-53). YOLO-v3 segments the input image using three mesh grids in different scales (i.e., 13×13 , 26×26 , 52×52). The model outputs detection on these three scales. Each grid contains three anchor boxes, whose dimensions are obtained by K-means clustering on the dimensions of ground truth bounding boxes. Each grid outputs three bounding box predictions. Henceforth, there are totally 10647 bounding boxes in the output of YOLO-v3. The Darknet-53 backbone outputs a feature map which contains bounding box parameters, box confidence, and object class probabilities. Specifically, for each bounding box, the feature map includes its height t_h , width t_w , center coordinates (t_x, t_y) , as well as class probabilities p_1, p_2, \dots, p_n and the objectness t_0 . t_0 is the confidence that a box contains an object. Given the feature map, the position of each detection box is then calculated based on anchor box dimension priors p_w and p_h , and centre offsets (c_x, c_y) from the top-left corner of the image. The final box dimension and position will then be:

$$\begin{aligned} b_x &= c_x + \theta(t_x) \\ b_y &= c_y + \theta(t_y) \\ b_w &= p_w e^{t_w} \\ b_h &= p_h e^{t_h} \end{aligned} \quad (6)$$

Herein, b_w is the box width, and b_h is the box height. b_x and b_y are the box center coordinates. The box confidence b_0 is calculated as:

$$b_0 = t_0 \cdot \max\{p_1, p_2, \dots, p_n\} \quad (7)$$

YOLO-v3 finally outputs the bounding boxes, the box confidences, and the class probabilities. The outputs will then be processed by NMS to generate the final detection results.

C. Non-Maximum Suppression (NMS)

NMS is integrated into object detection algorithms to filter detection boxes. NMS makes selections based on the Intersection over Union (IoU) between detection boxes. IoU measures the ratio of the overlapped area over the union area between two boxes. NMS works in two steps: 1) For a given object category, all of the detected bounding boxes in this category (i.e., candidate set) are sorted based on their box confidence scores from high to low; 2) NMS selects the box which has the highest box confidence score as the detection result, and then it discards other candidate boxes whose IoU value with the selected box is beyond the threshold. Then, within

the remaining boxes, NMS repeats the above two steps until there is no remaining box in the candidate set. Suppose the initial detection boxes are $B = b_1, b_2, \dots, b_n$, the corresponding box confidence scores are $S = s_1, s_2, \dots, s_n$. Given an NMS threshold N_t , we can write the NMS algorithm as Algorithm 1:

Algorithm 1: Non-Maximum Suppression

```

Input:  $B, S, N_t$ 
Initialisation:
 $D \leftarrow \{\}$ 
while  $B \neq \text{empty}$  do
   $m \leftarrow \text{argmax } S$ 
   $M \leftarrow b_m$ 
   $D \leftarrow D \cup B$ 
   $B \leftarrow B - M$ 
  for  $b_i \in B$  do
    if  $\text{IoU}(M, b_i) \geq N_t$  then
       $B \leftarrow B - b_i$ 
       $S \leftarrow S - s_i$ 
Output:  $D, S$ .

```

We can observe from the Algorithm 1 that NMS recursively discards the redundant detection boxes from the raw detection proposals B , until all raw proposals have been processed.

III. DAEDALUS ATTACK

We introduce our attack, namely Daedalus, in this section. To clarify the intuition behind the attack, we first analyse the vulnerability that we exploit to break NMS. Then, we introduce the general optimisation techniques used for making adversarial examples. Subsequently, we propose a series of adversarial loss functions to optimise in order to generate Daedalus adversarial examples. At last, we assemble the algorithms together to present the Daedalus attack, which can force a detection network to output an adversarial feature map that causes the malfunctioning of NMS.

A. Attacking NMS

We first introduce the vulnerability, which enables our attack, in NMS. NMS filters boxes based on the IoU between boxes. Specifically, after the raw detection boxes are obtained, the boxes with a confidence score below a given threshold will be discarded. Next, for a given object class and a box of this class with the highest box confidence score (i.e. the final detection box), NMS will discard other remaining boxes based on their IoUs with the final detection box. This mechanism makes NMS vulnerable to attacks that suppress the IoUs between output bounding boxes. Once the IoUs are suppressed below the required threshold for NMS filtering, NMS can no longer function normally. In this case, most of the redundant bounding boxes will be kept in the final detection results.

We consider three elemental schemes to break NMS. First, for algorithms such as YOLO-v3, it is necessary to make most of the bounding boxes survive the first round of filtering that discards boxes based on the box confidences. Hence, we need to maximise the box confidences. Second, to compress the IoUs, we can directly minimise the IoU for each pair of

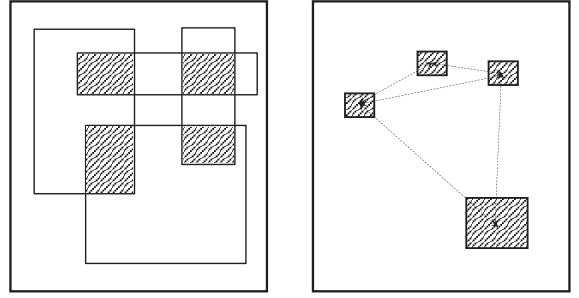


Fig. 2. The schemes we used to attack NMS. The scheme on the left side directly minimises IoUs between all box pairs. The second scheme takes a low-cost approximation of the first scheme. It minimises the dimension for all boxes, and maximises the Euclidean distance between box centres for all boxes.

boxes. Alternatively, we can minimise the expectation of the box dimension over all the bounding boxes, and maximise the expectation of the Euclidean distance between box centres over all pairs of boxes. The schemes are illustrated in Fig.2.

B. Generating adversarial example

We denote a benign example as x . An adversarial example of x is denoted as x' . The adversarial perturbation is $\delta = x' - x$. Therefore, the distortion calculated based on p -norm of the perturbation is $\|\delta\|_p$. We can then formulate the attack as the following optimisation problem:

$$\begin{aligned} \min_{\delta} \|\delta\|_p + c \cdot f(x + \delta) \\ \text{s.t. } x + \delta \in [0, 1]^n, \end{aligned} \quad (8)$$

wherein, f is an adversarial loss function. We will later select f from the loss functions presented in the previous section. c is a constant to balance the distortion and the adversarial loss f . δ is the adversarial perturbation. An adversary optimises δ to search for an adversarial example whose pixel values are bounded between 0 and 1. This is a typical box-constraint optimisation problem. To bound the pixel values of the generated adversarial examples between 0 and 1, we adopt the idea of changing variables from the paper [5]. We change the optimisation variables from δ to ω . There are different functions we can use for changing the variables (e.g. sigmoid function, arctan function, hyperbolic tangent function et. al). Among these functions, the hyperbolic tangent function generally produces higher gradients than others. Henceforth, to make the optimisation converge faster, we select the hyperbolic tangent function to change the variables. For δ_i in δ , we can apply a hyperbolic tangent function such that:

$$\delta_i = \frac{1}{2}(\tanh(\omega_i) + 1) - x_i. \quad (9)$$

We then optimise the above task based on the new variables ω . We apply binary search to find the best c during the optimisation. Finally, the adversarial perturbation δ can be calculated easily through the inverse of function 9.

C. Adversarial loss functions

In this section, we design loss functions that are used to find adversarial examples, which trigger malfunctioning of NMS. Based on the discussion in Section III-A, we formulate our attack into three potential adversarial loss functions. We will evaluate each loss function in Section IV. There are totally n detection boxes (in YOLO-v3, $n = 10647$). Supposing the object detector can be regarded as a function F . Given an input image x , the outputs are $F(x) = \{B^x, B^y, B^w, B^h, B^0, P\}$. Herein, $B^x = \{b_0^x, b_1^x, \dots, b_n^x\}$, $B^y = \{b_0^y, b_1^y, \dots, b_n^y\}$, $B^w = \{b_0^w, b_1^w, \dots, b_n^w\}$, and $B^h = \{b_0^h, b_1^h, \dots, b_n^h\}$. They are the dimensions and coordinates of the n output bounding boxes, as discussed in Section II-B. $B^0 = \{b_0^0, b_1^0, \dots, b_n^0\}$ are the objectness scores and $P = \{p_0, p_1, \dots, p_n\}$ are the class probabilities as introduced in Section II-B.

Our attack can specify an object classified as category λ to attack. If we want to attack multiple object categories, we can include these categories in a set Λ . Based on the above discussion, we define three loss functions, f_1 , f_2 , and f_3 , as follows:

$$f_1 = \frac{1}{\|\Lambda\|} \sum_{\lambda \in \Lambda} \mathbb{E}_{i: \text{argmax}(p_i) = \lambda} \{[b_i^0 \cdot \max(p_i) - 1]^2 + \mathbb{E}_{j: \text{argmax}(p_j) = \lambda} \text{IoU}_{ij}\}, \quad (10)$$

$$f_2 = \frac{1}{\|\Lambda\|} \sum_{\lambda \in \Lambda} \mathbb{E}_{i: \text{argmax}(p_i) = \lambda} \{[b_i^0 \cdot \max(p_i) - 1]^2 + \left(\frac{b_i^w \cdot b_i^h}{W \times H} \right)^2 + \mathbb{E}_{j: \text{argmax}(p_j) = \lambda} \frac{1}{(b_i^x - b_j^x)^2 + (b_i^y - b_j^y)^2}\}, \quad (11)$$

$$f_3 = \frac{1}{\|\Lambda\|} \sum_{\lambda \in \Lambda} \mathbb{E}_{i: \text{argmax}(p_i) = \lambda} \{[b_i^0 \cdot \max(p_i) - 1]^2 + \left(\frac{b_i^w \cdot b_i^h}{W \times H} \right)^2\}, \quad (12)$$

wherein, IoU_{ij} is the IoU between the i -th and the j -th bounding boxes. Box dimensions are scaled between 0 and 1 through dividing b^w and b^h by the input image width W and height H , such that the term is invariant towards changing input dimension.

In f_1 , we first minimise the expectation of mean squared error between the box confidence and 1 for all the boxes in which the detected objects are in the attacked category set Λ . Henceforth, the boxes will not be discarded due to low box confidence scores. In the second term, f_1 minimises the expectation of IoUs for all pairs of bounding boxes in Λ . The idea is straight forward. When the IoUs fall below the NMS threshold, the boxes can evade the NMS filter. Alternatively, we minimise the expectation of box dimensions and maximise the expectation of box distances in f_2 . f_2 approximates the effect of directly minimising IoU by compressing box dimensions and distributing boxes more evenly on the detected region.

Pairwise computation for obtaining IoUs and box distances could be expensive if the output feature map contains too many boxes. Therefore, we also propose f_3 as a more efficient loss function. f_3 only minimises the expectation of box dimensions instead of directly minimising the expectation of the IoUs. Minimising f_3 leads to smaller bounding boxes. When the boxes become small enough, there will be no intersection between the boxes. In other words, the IoUs between the boxes will be suppressed to zero. As a consequence, the boxes can avoid being filtered by NMS.

D. Daedalus attack against NMS

In this section, we assemble the above methods to form Daedalus attack. Actually, our attack can be applied to all FCN-based detectors. FCN-based detectors output the detected box dimension, box position and classification probabilities in a fully differentiable, end-to-end manner. Therefore, our attack can compute end-to-end adversarial gradients and optimise adversarial examples for FCN-based detectors. Herein, we present Daedalus attack based on YOLO-v3.

Algorithm 2: L_2 Daedalus attack

Input: $x, \Lambda, \gamma, \text{binary_steps}, \eta, \text{max_iteration}, c_{\max}, c_{\min}$
Initialisation:
 $c \leftarrow 10$
 $\text{loss}_{\text{init}} \leftarrow f(x)$
 $\delta \leftarrow 0$
 $x^* \leftarrow x + \delta$
for n starts from 0 to binary_steps **do**
 for i starts from 0 to max_iteration **do**
 select boxes in Λ to calculate loss $f(x^*)$
 $\delta \leftarrow \delta - \eta \nabla_{\delta} [\|\delta\| + c \cdot f(x^*)]$
 $x^* \leftarrow x^* + \delta$
 x' \leftarrow the best x^* found.
 if $f(x^*) \leq \text{loss}_{\text{init}} \cdot (1 - \gamma)$ **then**
 $c_{\max} = \min(c, c_{\max})$
 $c \leftarrow 0.5 \cdot (c_{\max} + c_{\min})$
 else
 $c_{\min} = \max(c, c_{\min})$
 $c \leftarrow 0.5 \cdot (c_{\max} + c_{\min})$
Output: Adversarial example x' .

Given an object detection task whose input is an image x , we are going to maximise the number of bounding box output from NMS. YOLO-v3 outputs three feature maps that are on different scales. The three feature maps are concatenated into one final feature map. The details of the YOLO-v3 feature map are discussed in Section II-B. We add a transformation layer after the feature map to obtain the final detection results. The transformation layer applies sigmoid transformations on the t_x and t_y in the feature map to get box centre coordinates b_x and b_y . Exponential transformations are applied on t_w and t_h to obtain box width b_w and box height b_h , respectively. We then calculate the values of the loss functions defined in Section III-C. Next, we minimise the loss value together with the distortion to generate our adversarial examples. During the optimisation, we introduce a hyper-parameter γ to control the strength of the attack.

Algorithm 3: L_0 Daedalus attack

Input: $x, \Lambda, \gamma, \text{binary_steps}, \eta, \text{max_iteration}, c_{\max}, c_{\min}$
Initialisation:
 $c \leftarrow 10$
 $loss_{\text{init}} \leftarrow f(x)$
 $\delta \leftarrow 0$
 $x^* \leftarrow x + \delta$
for n starts from 0 to binary_steps **do**
 for i starts from 0 to max_iteration **do**
 select boxes in Λ to calculate loss $f(x^*)$
 $\lambda = \text{argmax}_{\lambda \in \delta} \nabla_{\delta} [\|\delta\| + c \cdot f(x^*)]$
 $\delta \leftarrow \delta - \eta \nabla_{\lambda} [\|\delta\| + c \cdot f(x^*)]$
 $x^* \leftarrow x^* + \delta$
 end for
 $x' \leftarrow$ the best x^* found.
 if $f(x^*) \leq loss_{\text{init}} \cdot (1 - \gamma)$ **then**
 $c_{\max} = \min(c, c_{\max})$
 $c \leftarrow 0.5 \cdot (c_{\max} + c_{\min})$
 else
 $c_{\min} = \max(c, c_{\min})$
 $c \leftarrow 0.5 \cdot (c_{\max} + c_{\min})$
 end if
Output: Adversarial example x' .

We proposed our attack based on two distortion metrics, namely L_2 -norm and L_0 -norm. L_2 -norm and L_0 -norm are two representative distortion metrics. L_2 -norm attack limits the perturbations added on all the pixels, while L_0 -norm attack limits the total number of pixels to be altered. We develop these two versions of attack to study the effectiveness of all-pixel perturbation and selective-pixel perturbation while generating Daedalus adversarial examples.

For the L_2 Daedalus attack, we can directly minimise Equation 8. However, in L_0 Daedalus attack, since L_0 -norm is a non-differentiable metric, we alternatively select the pixels that have the highest adversarial gradients to perturb in each iteration, and then we clip other gradients to be 0. The detailed algorithm of L_2 Daedalus attack is presented in Algorithm 2, and the L_0 Daedalus attack is presented in Algorithm 3. Notice that Daedalus requires only the box parameters to launch the attack. This means that our attack can be applied to detection models that output feature maps which contain the geometry information of bounding boxes, even if they use different backbone networks.

IV. EVALUATION

We carried out experiments to evaluate the performance of our attacking approach. We ran our experiments on a server with four RTX 2080ti GPUs and 128G memory. The code of Daedalus attack can be obtained from <https://github.com/NeuralSec/Daedalus-attack>.

A. Experiment settings

In our evaluation, we selected YOLO-v3 as the model to attack. We first selected the best loss function, and then we quantified the performance of our attack, based on YOLO-v3 with NMS. We used YOLO-v3 as the substitutes to generate 416×416 adversarial perturbations in our experiments. During the binary search for finding the best constant c in our optimisation algorithm, we adjusted the number of maximal search step to 5.

We produced adversarial examples of images in the COCO 2017val dataset [29]. We generated adversarial examples using both our L_0 and L_2 attacks. For each attack, first, to investigate the effectiveness of different attacking confidence γ , we ranged γ from 0.1 to 0.9, and selected 10 COCO examples to perturb under each γ . Second, we randomly selected 100 COCO examples to perturb under both a low $\gamma = 0.3$ and a high $\gamma = 0.7$. To unify the results in our evaluation, we included all 80 object categories of COCO dataset in the object category set Λ to be attacked in our loss functions. We also selected object categories of 'person' and 'car' to attack. The results are demonstrated in the appendix.

To prove that our attack can be applied to different detectors, we also demonstrate attacking RetinaNet-ResNet-50 in the paper. RetinaNet-ResNet-50 uses ResNet-50 [19] as the backbone. The backbone differs from that of YOLO-v3. The output feature map is different as well. In this way, we demonstrate that our Daedalus adversarial example can attack against detectors with different backbone structures. Moreover, we studied the attack in the black-box scenario by using an ensemble of substitutes in our attack to craft robust adversarial examples. The visualisations of the detection results are presented in the appendix.

B. Loss function selection

We proposed three adversarial loss functions to craft adversarial examples (Equations 10, 11, and 12). We compared these three loss functions, and select the best loss function in this section. We selected 10 random images from COCO dataset. Based on each function, we generated 416×416 sized adversarial examples of these 10 images. We recorded the runtime per example and the volatile GPU utilisation of each loss functions. We measured the performance of each function by looking at the success rate of finding adversarial examples at different attacking confidence. Since our L_0 attack essentially has the same optimisation process with that of L_2 , we only ran our L_2 attack for the comparison in this section. The results are recorded in Table I.

The recorded runtime was averaged from the runtime of generating all the examples under the loss function. The GPU utilisation was also averaged from running all examples. We only used one GPU to generate adversarial example in this section. It can be observed that f_3 (i.e. Equation 12) has the best success rate of finding adversarial examples under different confidence γ . Moreover, f_3 has the shortest runtime and the lowest GPU utilisation compared to f_1 and f_2 .

Based on the comparison, we select f_3 , which is simple but effective, as the loss function for Daedalus attack. We continue evaluating Daedalus attack in the following sections based on f_3 (Equation 12).

C. Quantitative performance

In this section, we evaluated our attack from two aspects. First, we evaluated how would Daedalus attack perform under different NMS thresholds. Second, we investigated how would the confidence γ of attack affect the detection results. We

TABLE I
LOSS FUNCTION COMPARISON

Loss Function	Metric	Value of γ								
		0.1	0.2	0.3	0.4	0.5	0.6	0.7	0.8	0.9
f_1	Runtime					2375.62 s				
	GPU-Util					79%				
	Success rate	100%	100%	100%	90%	40%	40%	20%	0%	0%
f_2	Runtime					1548.57 s				
	GPU-Util					77%				
	Success rate	100%	100%	100%	100%	100%	90%	40%	20%	0%
f_3	Runtime					1337.06 s				
	GPU-Util					73%				
	Success rate	100%	100%	100%	100%	100%	100%	70%	40%	40%

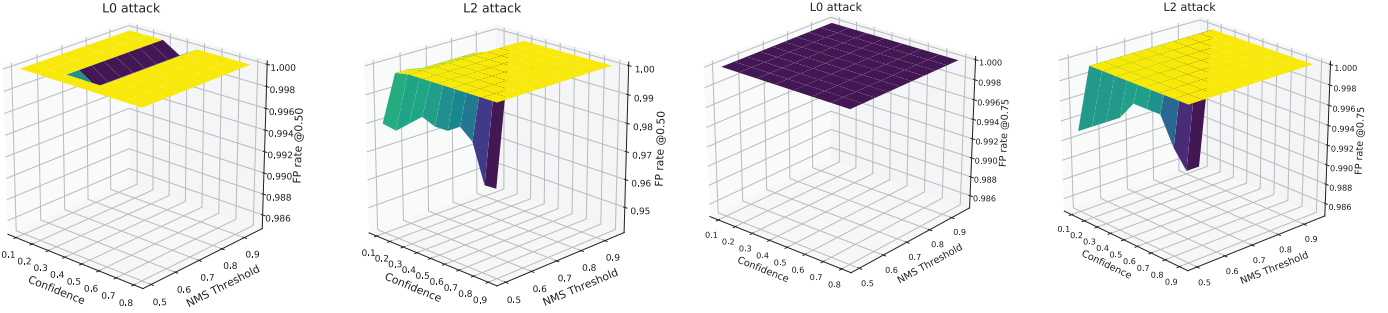


Fig. 3. The false positive rate at IoU threshold of 0.5 with respect to NMS threshold and confidence of attack. The NMS threshold ranges from 0.5 to 0.95. The confidence ranges from 0.1 to 0.9 in L_2 attack, 0.1 to 0.8 in L_0 attack. Each FP rate is averaged from the FP rates of 10 Daedalus examples.

assessed the performance of our adversarial example on a YOLO-v3 detector. Herein, we quantified the attack performance based on three metrics: False Positive (FP) rate, mean average precision (mAP), and distortion of the example.

First, to investigate the effect of NMS threshold on our attack, we obtained the detection results of each adversarial/benign example under a series of NMS thresholds, which ranged between 0.5 and 0.95. Second, to assess the effect of confidence γ on the performance of the attack, we crafted adversarial examples under confidences from 0.1 to 0.9.

False positive rate. In order to quantify the performance of our attack, we measured the False Positive (FP) rate of detecting Daedalus example. The FP rate is defined as the ratio of false positive detection boxes with respect to the total number of detection boxes. FP rate can be defined as follows:

$$FP \text{ rate} = \frac{N_\phi + 1}{N + 1}, \quad (13)$$

wherein N_ϕ is the number of false positive detection boxes, and N is the total number of bounding boxes. We add 1 to both the numerator and the denominator to avoid ill definition when there is no detected bounding box. FP rate measures the proportion of redundant boxes that are not filtered by NMS. FP rate equals 1 when there is no correct detection result.

We varied the IoU threshold in NMS from 0.5 to 0.95 in every 0.05 to obtain detection outputs under different thresholds. We then obtained the detection results of Daedalus

Fig. 4. The false positive rate at IoU threshold of 0.75 with respect to NMS threshold and confidence of attack. The NMS threshold ranges from 0.5 to 0.95. The confidence ranges from 0.1 to 0.9 in L_2 attack, 0.1 to 0.8 in L_0 attack. Each FP rate is averaged from the FP rates of 10 Daedalus examples.

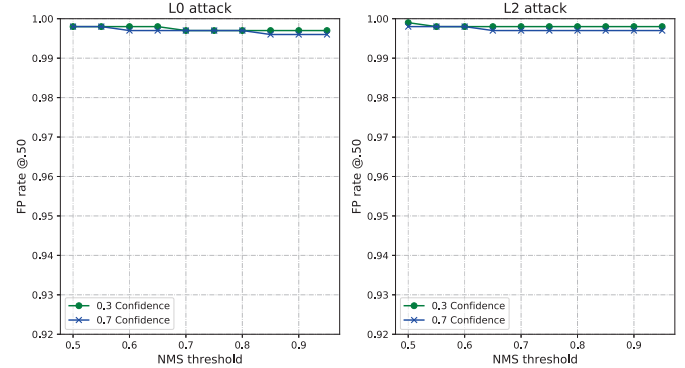


Fig. 5. L_0 attack false positive rate at IoU threshold of 0.5 with respect to NMS threshold. Each FP rate is averaged from the detection results of 100 Daedalus examples.

examples made under confidences from 0.1 to 0.9 (0.1 to 0.8 for L_0 attack since it could not find examples of 0.9 confidence). This is because the L_0 attack could not further discard perturbations from L_2 examples under a high γ . We then recorded the FP rates of the detection results based on IoU thresholds of 0.5 and 0.75 in Fig.3 and Fig.4, respectively. Each FP rate is averaged from 10 Daedalus examples. We then measured the average FP rate of the 100 examples crafted under confidence of 0.3/0.7. We plotted the trends of the average FP rate at IoU threshold of 0.5 and 0.75 with respect to NMS threshold in Fig.5 and Fig.6, respectively.

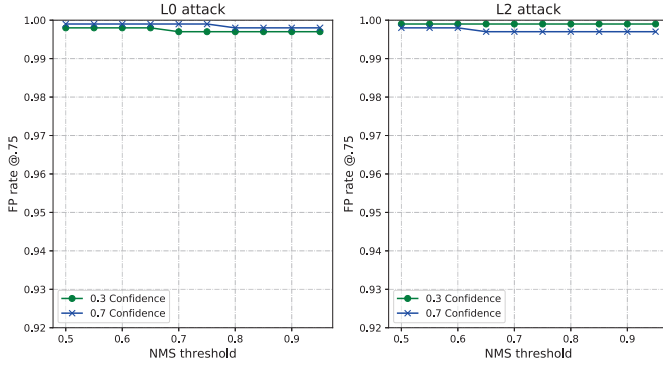


Fig. 6. L_0 attack false positive rate at IoU threshold of 0.75 with respect to NMS threshold. Each FP rate is averaged from the detection results of 100 Daedalus examples.

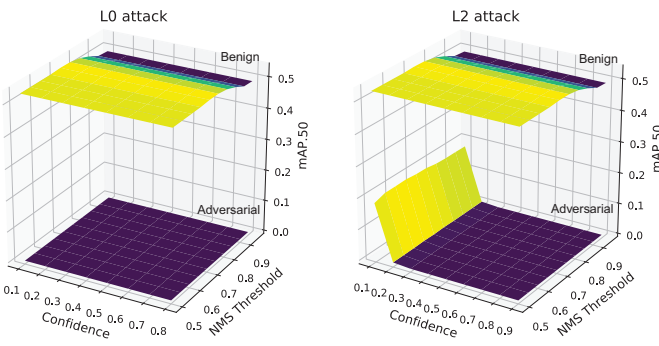


Fig. 7. $mAP^{IoU=0.50}$ of Daedalus example detection results with respect to NMS threshold and attack confidence. The threshold ranges from 0.5 to 0.95. Each mAP is averaged from the detection results of 10 Daedalus examples.

It can be observed that both L_0 and L_2 attacks had achieved above 90% of FP rate under different NMS thresholds, even with the lowest attack confidence of 0.1. Increasing NMS threshold can slightly reduce the FP rate of the low confidence attacks. However, changing NMS threshold barely had an impact on the performance of high confidence attacks. FP rate increased with increasing confidence of attack. Almost 99.9% of the detected objects were false positive given a high confidence Daedalus example, even with a high NMS threshold.

Mean average precision. In this part, we investigated how would our adversarial example change the mAP of detection results. The mAP is commonly used to evaluate the performance of object detection model. Therefore, mAP averages the Average Precisions (AP s) over all detected object categories. It is defined as follows:

$$mAP = \frac{1}{M} \sum_{i \in \{1, 2, \dots, M\}} AP_i, \quad (14)$$

wherein M is the number of object category. We adopted all-point interpolation AP from Pascal VOC challenge [11] to calculate mAP .

We used the recommended COCO evaluation metrics $mAP^{IoU=0.50}$ and $mAP^{IoU=0.75}$, which are the mAP s cal-

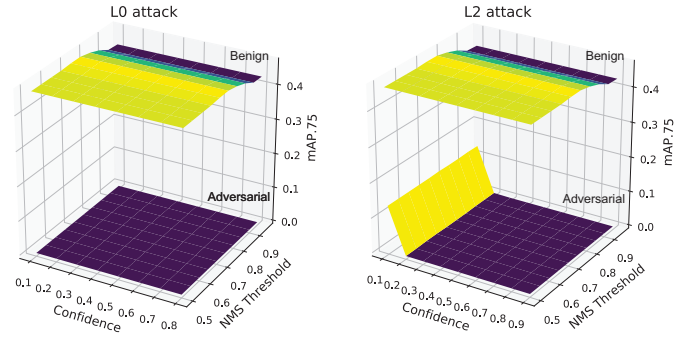


Fig. 8. $mAP^{IoU=0.75}$ of Daedalus example detection results with respect to NMS threshold and attack confidence. The threshold ranges from 0.5 to 0.95. Each mAP is averaged from the detection results of 10 Daedalus examples.

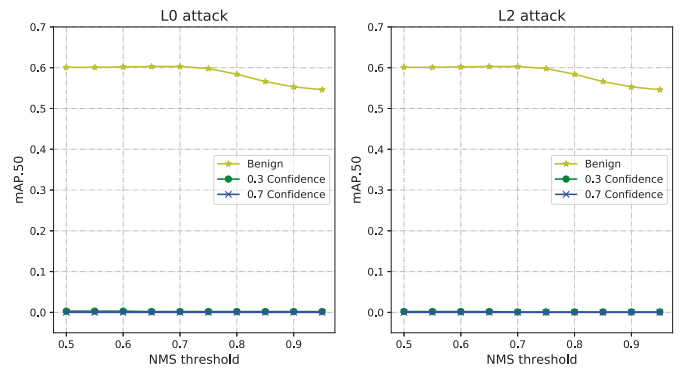


Fig. 9. $mAP^{IoU=0.50}$ of L_0 and L_2 Daedalus attacks with respect to NMS threshold. The threshold ranges from 0.5 to 0.95. Each mAP is averaged from the detection results of 100 Daedalus examples.

culated at IoU thresholds of 0.5 and 0.75, to evaluate the detection precisions on benign examples and Daedalus examples. We varied the NMS threshold and the confidence of attack to obtain the mAP s of the detection results. The results are displayed in Fig.7 and Fig.8. We also summarised the average $mAP^{IoU=0.50}$ and $mAP^{IoU=0.75}$ of the 100 examples made under confidence of 0.3 and 0.7 in Fig.9 and Fig.10, respectively.

Based on the evaluation results, both our L_0 and L_2 attacks decreased the mAP of the detector from 45% ~ 59% to a value between 0% to 17.8%. The mAP dropped to 0% when the confidence of the attack passed 0.2.

Distortion of the examples. We evaluated the distortion of the Daedalus adversarial examples crafted based on L_2 -norm and L_0 -norm. For a fair comparison, the distortions are measured using L_2 -norm. We recorded the maximum, the minimum and the average distortion of 10 adversarial examples under each attacking confidence. The results are summarised in Table II. It can be found that the distortion of adversarial examples has a positive correlation with the confidence of attack. The distortion increases slowly before the confidence reaches 0.6. Once the confidence surpasses 0.6, there is a rapid increase in the distortion level. Additionally, compared to L_2 attack, L_0 could not find adversarial examples at a confidence of 0.9.

TABLE II
DISTORTIONS UNDER DIFFERENT CONFIDENCES

Attack	Distortion	Value of γ								
		0.1	0.2	0.3	0.4	0.5	0.6	0.7	0.8	0.9
L_2 Daedalus	Maximum	157.49	259.25	113.24	324.53	598.45	4138.47	5915.90	25859.67	19553.05
	Average	130.59	218.86	96.51	166.27	344.75	1670.35	1835.04	9953.59	14390.76
	Minimum	94.30	175.07	75.24	95.30	185.25	351.55	366.49	210.24	11894.38
L_0 Daedalus	Maximum	162.74	513.54	555.11	1200.48	1001.86	42144.96	3891.80	3364.29	N/A
	Average	87.81	346.71	440.21	651.77	736.40	12765.82	1992.30	1501.58	N/A
	Minimum	53.26	165.50	339.44	402.48	436.15	3713.67	729.38	848.36	N/A

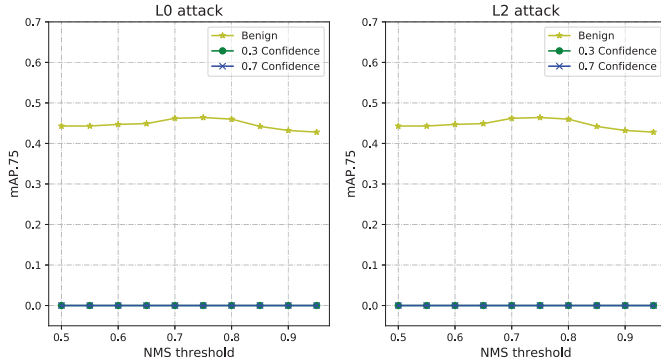


Fig. 10. $mAP^{IoU=.75}$ of L_0 and L_2 Daedalus attacks with respect to NMS threshold. The threshold ranges from 0.5 to 0.95. Each mAP is averaged from the detection results of 100 Daedalus examples.

Based on the evaluation, both L_0 and L_2 attacks require reasonable distortions for making low-confidence examples. Compared to the L_0 attack, our L_2 attack introduced less distortion when the confidence is between 0.2 and 0.7, and the L_2 attack was slightly better in terms of finding adversarial examples under confidence of 0.9. However, the L_0 attack could reduce the distortion when the confidence surpassed 0.8. Consider that FCN based object detectors usually segment the input image by a mesh grid. Each grid has its own responsibility for detecting objects. Low-level perturbation based on L_0 -norm may leave some of the grids unperturbed. Therefore, these grids can still output normal detection results, which can be filtered by NMS. As a consequence, the L_0 attack attempts to perturb most of the pixels to generate a qualified adversarial example, which leads to high distortion on the example. High-level perturbation was imposed on each pixel when the confidence went over 0.8. In return, our L_0 attack can discard the perturbation on some pixels to reduce the overall distortion.

V. ANALYSIS OF OUR ATTACK

In this section, we first investigate whether our attack can be extended to a variation of NMS algorithm, namely soft-NMS. Second, we demonstrated applying Daedalus attack to attack RetinaNet-Resnet-50. Third, we propose using an ensemble of substitutes to make robust Daedalus examples that can attack multiple object detectors. The proposed ensemble attack grants transferability to Daedalus examples, such that an attacker can

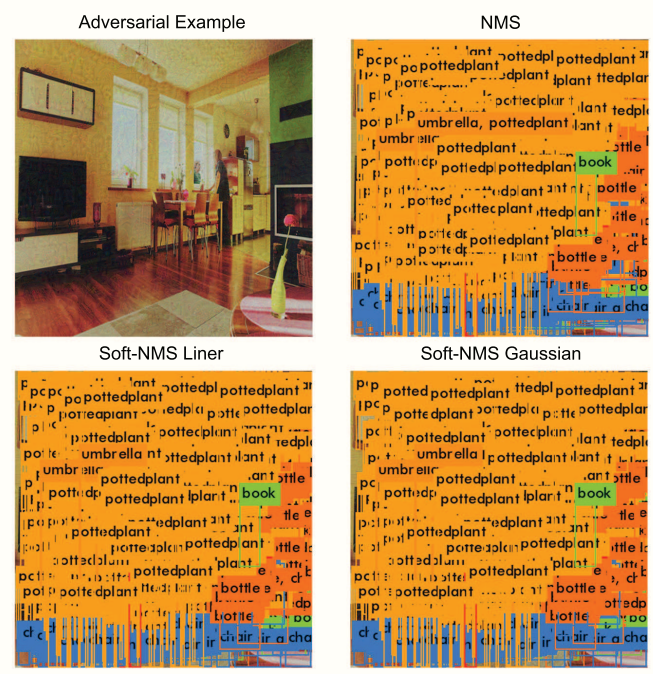


Fig. 11. Daedalus attack against soft-NMS. The top left image is an L_0 Daedalus example crafted under a confidence of 0.3. The top right one shows the detection results from NMS, as a reference. The left bottom one shows the results of linear soft-NMS, and the right bottom one shows the results of Gaussian soft-NMS.

launch the attack in a black-box scenario. At last, we discuss the dilemma of defending against Daedalus attack.

A. Breaking Soft-NMS

Apart from breaking NMS, we also tested our attack on soft-NMS, which iteratively decreases the confidence score of overlapping boxes instead of discarding the boxes [3]. Soft-NMS has both linear version and Gaussian version. We applied our attack on both versions to investigate whether soft-NMS can handle our attack. We randomly selected an L_0 and L_2 Daedalus examples to attack a soft-NMS-equipped YOLO-v3 detector. The detection results of the L_0 adversarial examples are displayed in Fig.11, and the detection results of the L_2 adversarial examples are illustrated in Fig.12. We can find that both our L_0 and L_2 attacks broke linear soft-NMS and Gaussian soft-NMS.

We also evaluated the FP rate of our attack against soft-NMS. The results are shown in Fig.13. From the figure, we

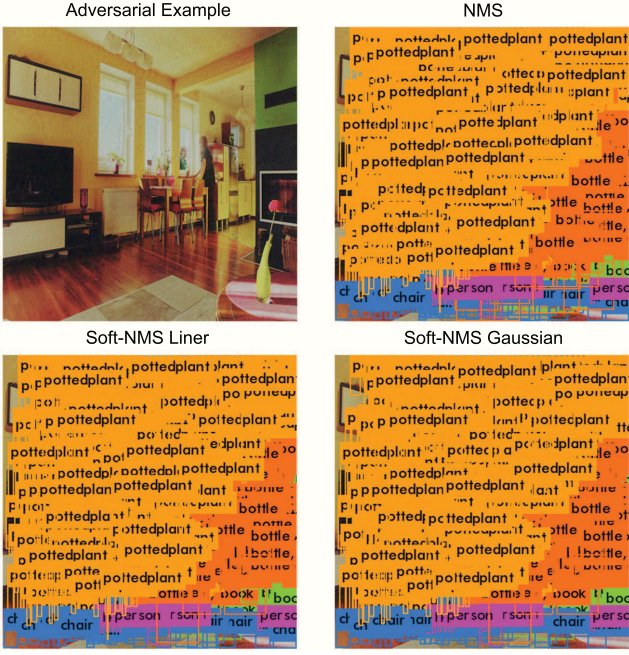


Fig. 12. Daedalus attack against soft-NMS. The top left image is an L_2 Daedalus example crafted under a confidence of 0.3. The top right one shows the detection results from NMS, as a reference. The left bottom one shows the results of linear soft-NMS, and the right bottom one shows the results of Gaussian soft-NMS.

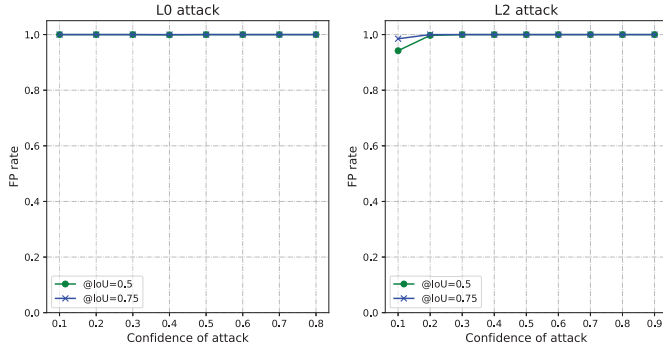


Fig. 13. The FP rate of Daedalus attack against YOLO-v3 with soft-NMS. We evaluated the FP rate at IoU thresholds of 0.5 and 0.75.

can observe that our attack broke soft-NMS as well. Our L_0 adversarial examples made under different confidence resulted in 100% FP rate. Our L_2 attack led to 100% FP rate when the attack confidence went over 0.2.

B. Attacking RetinaNet

The Daedalus attack can be applied to different FCN-based detection algorithms. To demonstrate this capability, we applied the Daedalus attack on another popular object detection algorithm, RetinaNet [28]. By default, we selected ResNet-50 as the backbone network of RetinaNet. RetinaNet extracts the feature maps which contain the features of detection boxes and object classes by using a feature pyramid network (FPN) [27]. The features will then be processed by regression models to obtain the position and the dimension of the bounding boxes.

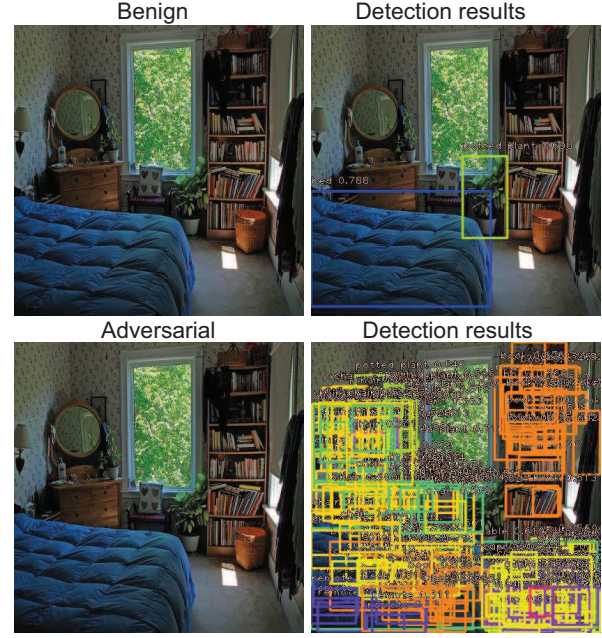


Fig. 14. The detection results of a Daedalus adversarial example made by our L_2 attack towards RetinaNet-ResNet-50.

The object classification results will be obtained from the feature maps by classification models.

We followed the same procedure of attacking YOLO-v3 to attack RetinaNet. We calculated the adversarial loss based on Equation 12, and generate adversarial examples based on optimising Equation 8. We only tested our L_2 attack since a succeeded L_2 attack guarantees a successful L_0 attack, according to the mechanism of the attacks. We generated 10 416×416 adversarial examples under confidence of 0.3. We plotted one of the detection results from RetinaNet in Fig.14. It can be observed that the example triggered malfunctioning of NMS in RetinaNet, and led to extremely dense detection results.

We also measured the FP rate and the mAP of the RetinaNet detection results on the 10 Daedalus examples. The FP rate with respect to NMS threshold is plotted in Fig.15. The mAP with respect to NMS threshold is plotted in Fig.16. More detection results of Daedalus examples from RetinaNet are presented in the appendix.

It can be observed from Fig.15 that Daedalus attack stimulated the FP rate of RetinaNet above 99%. According to Fig.16, our attack decreased $mAP^{IoU=.50}$ of RetinaNet from around 0.27 to below 0.05. $mAP^{IoU=.75}$ was decreased to 0. Our attack is effective against RetinaNet.

C. Ensemble of substitutes

The transferability of misclassification adversarial examples has been investigated in the paper [18]. However, instead of causing misclassification, our attack takes a different attacking purpose (i.e. disabling NMS). Hence, the transferability of our Daedalus adversarial example may demonstrate totally differ-

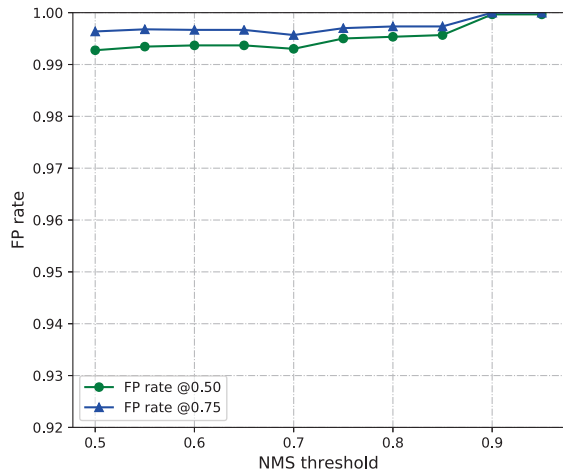


Fig. 15. $FP\ rate^{IoU=.50}$ and $FP\ rate^{IoU=.75}$ of our L_2 Daedalus attack against RetinaNet, with respect to NMS threshold. The NMS threshold ranges from 0.5 to 0.95. Each FP rate is averaged from the detection results of 10 Daedalus examples.

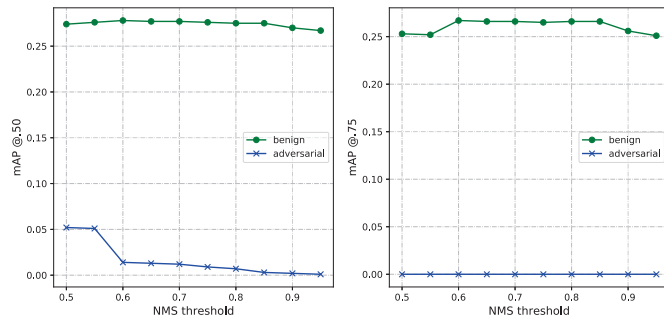


Fig. 16. $mAP^{IoU=.50}$ and $mAP^{IoU=.75}$ of our L_2 Daedalus attacks against RetinaNet, with respect to NMS threshold. The threshold ranges from 0.5 to 0.95. Each mAP is averaged from the detection results of 10 Daedalus examples.

ent properties compared to the misclassification of adversarial examples.

To launch the black-box attack using Daedalus, we suggest using an ensemble of popular object detection models as the substitute to generate adversarial examples. The intuition behind is largely based on the fact that current object detection algorithms have very limited types of backbone networks. The popular backbones and detection model are often reused in different systems [30]. To make robust examples that can transfer among different models, we can construct the substitute using multiple different backbone networks. We assembled darknet-53 and Resnet-50 together, in parallel, as the substitute to craft Daedalus adversarial examples. Given an input perturbation, it aims to break NMS in both detection models. To do so, we simply concatenated the detected box dimension values from the two models, and then we optimised the perturbation based on the expectation of the output box dimensions over the two models. In other words, we modified the loss function from f_3 to Equation 15:

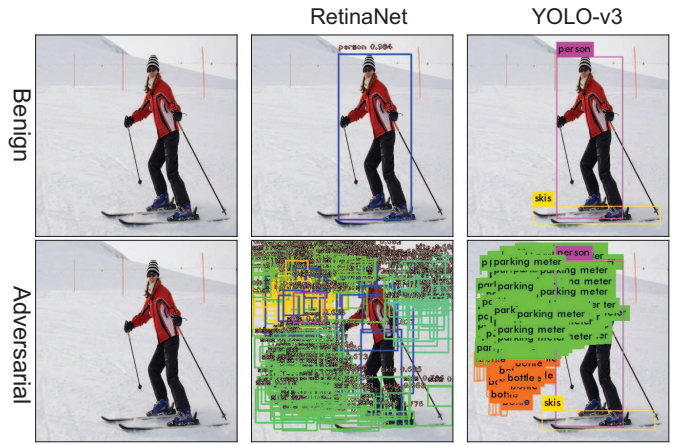


Fig. 17. The detection results of a Daedalus adversarial example made by ensemble-of-substitutes approach. We tested the transferability by detecting the adversarial example using both YOLO-v3 and RetinaNet. The first row contains a benign example and the detection results from RetinaNet and YOLO-v3. The second row contains the adversarial example and the detection results of the adversarial example.

$$f = \mathbb{E}_{m \sim M} f_3^m, \quad (15)$$

herein, M is an ensemble of substitutes, which includes the possible object detection models. f_3^m is the loss value of a model m in M , calculated based on f_3 (i.e. Equation 12). We tested our ensemble-of-substitutes attack on both YOLO-v3 and RetinaNet to observe transferability. We crafted an adversarial example based on the ensemble method, and then we tested the example on YOLO-v3 and RetinaNet. YOLO-v3 uses Darknet-53 as the backbone network. In contrast, RetinaNet has a different backbone network (ResNet). Henceforth, RetinaNet extracts feature map that is distinct from that of YOLO series. The detection results of the adversarial example from both YOLO-v3 and RetinaNet are displayed in Fig.17. We can observe that the adversarial example can trigger NMS malfunctioning for both YOLO-v3 and RetinaNet. The detection results for more adversarial examples crafted using ensemble of substitutes can be found in the appendix of this paper.

D. Discussion of Daedalus attack

Adversarial examples were firstly proposed towards machine learning classifiers. Hence, current defending methods focus on classification tasks. Defences can be categorised into either reactive defence (e.g. [15], [32], [36], [38], [39], [54], [58]), or proactive defence (e.g. [7], [8], [17], [35], [37], [44], [52], [55], [56]). For most of the reactive defence methods, a second model is adopted to detect examples with adversarial perturbation. In the category of proactive defence, a model is trained to be robust towards adversarial examples. Currently, there is no defending method proposed towards the new type of attack introduced by Daedalus example.

Daedalus attack poses an intimidating threat to object detection tasks. Current machine learning tasks, especially object

detection tasks, are commonly developed by reusing existing model [24]. Therefore, an adversary can first adopt an ensemble of substitutes to launch the attack in black-box settings by including popular backbone networks in the ensemble of substitutes. Second, an adversary can pre-guess the type of the backbone network and then launch the attack. Unlike attacks against the machine learning classifiers, Daedalus attack compresses the box dimension values in the feature map to undermine the NMS functionality. **Limiting the minimal size of detection boxes can possibly mitigate Daedalus attack. However, this would also reduce the performance of the detection algorithm towards small objects.** This dilemma makes defending against Daedalus attack a difficult task.

As revealed by our attack, NMS is no longer a secure solution for object detection. Based on our evaluation in Section IV, changing NMS threshold cannot prevent our attack from breaking NMS either. We may need to propose new algorithms to filter redundant bounding boxes for object detection task if there had no effective defence been proposed towards Daedalus attack.

VI. RELATED WORK

Methods for crafting adversarial examples against classification tasks have been extensively studied. The basic algorithms for generating examples can be divided into gradient based attacks and forward derivative based attack. Gradient-based attacks find adversarial examples by minimising the cost of the adversarial objective set by the attacker, based on gradient descent. For example, L-BFGS was adopted to optimise the adversarial objective functions for generating adversarial examples [5], [55]. Fast gradient sign method was proposed to rapidly find first-order Taylor polynomial approximations of adversarial examples based on gradient descent or gradient sign descent [14]. Basic iterative method relies on multiple steps of gradient descent to generate adversarial examples [26]. Deepfool computes adversarial gradients based on the local linearity of neural networks [40]. Forward derivative based attack perturbs salient features based on the Jacobian between the model inputs and outputs [43]. Based on these algorithms, there are evolved attacks that use different distortion metrics to make adversarial examples that are more imperceptible for human beings [10], [23]. Furthermore, there are methods proposed to craft adversarial example of data that has discrete features (e.g. text) [9], [16], [25].

Beyond the above attacks, some methods can generate robust adversarial examples which can fool real-world classifiers and detectors. For example, dense adversarial generation (DAG) algorithm was proposed to craft adversarial example for object detection and segmentation [57]. Lu et al. craft robust adversarial examples that cause misclassification of object detector [33]. RP_2 was proposed to craft adversarial example of real-world road signs [12]. Subsequently, RP_2 was extended to attack YOLO-v2 [53]. Recently, expectation over transformation (EoT) algorithm was proposed to synthesise robust adversarial examples [2], [4]. However, current adversarial examples only focus on triggering misclassification

in machine learning classifiers/object detectors. Our Daedalus attack creates adversarial examples that lead to malfunctioning of NMS, which is different from all the previous attacks.

VII. CONCLUSION

In this paper, we propose a novel type of adversarial example which aims at disabling NMS in object detection models. The proposed attack, Daedalus, can control both the strength of the generated adversarial examples and the object class to attack. The attacked model will output extremely noisy detection result such that the detection service is no longer functional. Our attack can reduce the mAP of the detection to nearly 0%. The FP rate of detecting the Daedalus examples can go up to 99.9%. Meanwhile, the required distortion to make Daedalus attack is imperceptible. Daedalus attack aims at breaking NMS instead of causing misclassification. Unlike defending misclassification adversarial examples, it is difficult to defend against such attack since the attacked feature map is much more complicated than classification logits. The transferability of the proposed Daedalus attack is affected by the selected substitutes while launching the attack. We rely on minimising the expectation of box dimensions over a set of feature maps to make robust examples, which can make NMS malfunction in multiple detection models. There are some remaining problems we aim to address in future. First, considering the complexity of object detection feature maps, it is difficult to make universal adversarial examples that can launch zero-knowledge attacks. Second, Daedalus attack reveals a vulnerability in object detection, which can cause fatal consequence in the real world. Nevertheless, defending method against Daedalus attack is still a missing piece. We will address these problems in our future work.

REFERENCES

- [1] N. Akhtar and A. Mian. Threat of adversarial attacks on deep learning in computer vision: A survey. *IEEE Access*, 6:14410–14430, 2018.
- [2] A. Athalye and I. Sutskever. Synthesizing robust adversarial examples. *arXiv preprint arXiv:1707.07397*, 2017.
- [3] N. Bodla, B. Singh, R. Chellappa, and L. S. Davis. Soft-nmsimproving object detection with one line of code. In *Computer Vision (ICCV), 2017 IEEE International Conference on*, pages 5562–5570. IEEE, 2017.
- [4] T. B. Brown, D. Mané, A. Roy, M. Abadi, and J. Gilmer. Adversarial patch. *arXiv preprint arXiv:1712.09665*, 2017.
- [5] N. Carlini and D. Wagner. Towards evaluating the robustness of neural networks. In *2017 IEEE Symposium on Security and Privacy (SP)*. IEEE, may 2017.
- [6] Z. Chen, S. Huang, and D. Tao. Context refinement for object detection. In *The European Conference on Computer Vision (ECCV)*, September 2018.
- [7] M. Cisse, P. Bojanowski, E. Grave, Y. Dauphin, and N. Usunier. Parseval networks: Improving robustness to adversarial examples. In *International Conference on Machine Learning*, pages 854–863, 2017.
- [8] G. S. Dhillon, K. Azizzadenesheli, Z. C. Lipton, J. Bernstein, J. Kossaifi, A. Khanna, and A. Anandkumar. Stochastic activation pruning for robust adversarial defense. *arXiv preprint arXiv:1803.01442*, 2018.
- [9] J. Ebrahimi, A. Rao, D. Lowd, and D. Dou. Hotflip: White-box adversarial examples for text classification. In *Proceedings of ACL*, 2018.
- [10] L. Engstrom, D. Tsipras, L. Schmidt, and A. Madry. A rotation and a translation suffice: Fooling cnns with simple transformations. *arXiv preprint arXiv:1712.02779*, 2017.
- [11] M. Everingham, L. Van Gool, C. K. Williams, J. Winn, and A. Zisserman. The pascal visual object classes (voc) challenge. *International journal of computer vision*, 88(2):303–338, 2010.

[12] I. Evtimov, K. Eykholt, E. Fernandes, T. Kohno, B. Li, A. Prakash, A. Rahmati, and D. Song. Robust physical-world attacks on machine learning models. *arXiv preprint arXiv:1707.08945*, 2(3):4, 2017.

[13] R. Girshick. Fast r-cnn. In *Proceedings of the IEEE international conference on computer vision*, pages 1440–1448, 2015.

[14] I. J. Goodfellow, J. Shlens, and C. Szegedy. Explaining and harnessing adversarial examples. *Computer Science*, 2014.

[15] K. Grosse, P. Manoharan, N. Papernot, M. Backes, and P. McDaniel. On the (statistical) detection of adversarial examples. *arXiv preprint arXiv:1702.06280*, 2017.

[16] K. Grosse, N. Papernot, P. Manoharan, M. Backes, and P. McDaniel. Adversarial examples for malware detection. In *European Symposium on Research in Computer Security*, pages 62–79. Springer, 2017.

[17] S. Gu and L. Rigazio. Towards deep neural network architectures robust to adversarial examples. *Computer Science*, 2015.

[18] R. Gurbaxani and S. Mishra. Traits & transferability of adversarial examples against instance segmentation & object detection. *arXiv preprint arXiv:1808.01452*, 2018.

[19] K. He, X. Zhang, S. Ren, and J. Sun. Deep residual learning for image recognition. In *Proceedings of the IEEE conference on computer vision and pattern recognition*, pages 770–778, 2016.

[20] P. Henderson and V. Ferrari. End-to-end training of object class detectors for mean average precision. In *Asian Conference on Computer Vision*, pages 198–213. Springer, 2016.

[21] J. Hosang, R. Benenson, and B. Schiele. A convnet for non-maximum suppression. In *German Conference on Pattern Recognition*, pages 192–204. Springer, 2016.

[22] J. H. Hosang, R. Benenson, and B. Schiele. Learning non-maximum suppression. In *CVPR*, pages 6469–6477, 2017.

[23] H. Hosseini and R. Pooventrakul. Semantic adversarial examples. In *Proceedings of the IEEE Conference on Computer Vision and Pattern Recognition Workshops*, pages 1614–1619, 2018.

[24] Y. Ji, X. Zhang, S. Ji, X. Luo, and T. Wang. Model-reuse attacks on deep learning systems. In *Proceedings of the 2018 ACM SIGSAC Conference on Computer and Communications Security*, pages 349–363. ACM, 2018.

[25] R. Jia and P. Liang. Adversarial examples for evaluating reading comprehension systems. In *Proceedings of the 2017 Conference on Empirical Methods in Natural Language Processing*, pages 2021–2031, 2017.

[26] A. Kurakin, I. Goodfellow, and S. Bengio. Adversarial examples in the physical world. *arXiv preprint arXiv:1607.02533*, 2016.

[27] T.-Y. Lin, P. Dollár, R. Girshick, K. He, B. Hariharan, and S. Belongie. Feature pyramid networks for object detection. In *CVPR*, volume 1, page 4, 2017.

[28] T.-Y. Lin, P. Goyal, R. Girshick, K. He, and P. Dollár. Focal loss for dense object detection. *IEEE transactions on pattern analysis and machine intelligence*, 2018.

[29] T.-Y. Lin, M. Maire, S. Belongie, J. Hays, P. Perona, D. Ramanan, P. Dollár, and C. L. Zitnick. Microsoft coco: Common objects in context. In *European conference on computer vision*, pages 740–755. Springer, 2014.

[30] L. Liu, W. Ouyang, X. Wang, P. Fieguth, J. Chen, X. Liu, and M. Pietikäinen. Deep learning for generic object detection: A survey. *arXiv preprint arXiv:1809.02165*, 2018.

[31] W. Liu, D. Anguelov, D. Erhan, C. Szegedy, S. Reed, C.-Y. Fu, and A. C. Berg. Ssd: Single shot multibox detector. In *European conference on computer vision*, pages 21–37. Springer, 2016.

[32] J. Lu, T. Issaranon, and D. Forsyth. Safetynet: Detecting and rejecting adversarial examples robustly. *arXiv preprint arXiv:1704.00103*, 2017.

[33] J. Lu, H. Sibai, and E. Fabry. Adversarial examples that fool detectors. *arXiv preprint arXiv:1712.02494*, 2017.

[34] K. Lu, X. An, J. Li, and H. He. Efficient deep network for vision-based object detection in robotic applications. *Neurocomputing*, 245:31–45, 2017.

[35] C. Lyu, K. Huang, and H.-N. Liang. A unified gradient regularization family for adversarial examples. In *Data Mining (ICDM), 2015 IEEE International Conference on*, pages 301–309. IEEE, 2015.

[36] X. Ma, B. Li, Y. Wang, S. M. Erfani, S. Wijewickrema, M. E. Houle, G. Schoenebeck, D. Song, and J. Bailey. Characterizing adversarial subspaces using local intrinsic dimensionality. *arXiv preprint arXiv:1801.02613*, 2018.

[37] A. Madry, A. Makelov, L. Schmidt, D. Tsipras, and A. Vladu. Towards deep learning models resistant to adversarial attacks. *arXiv preprint arXiv:1706.06083*, 2017.

[38] D. Meng and H. Chen. Magnet: a two-pronged defense against adversarial examples. *arXiv preprint arXiv:1705.09064*, 2017.

[39] J. H. Metzen, T. Genewein, V. Fischer, and B. Bischoff. On detecting adversarial perturbations. In *The 5th IEEE International Conference on Learning Representation*, 2017.

[40] S. M. Moosavidezfooli, A. Fawzi, and P. Frossard. Deepfool: A simple and accurate method to fool deep neural networks. In *IEEE Conference on Computer Vision and Pattern Recognition*, pages 2574–2582, 2016.

[41] A. Neubeck and L. Van Gool. Efficient non-maximum suppression. In *Pattern Recognition, 2006. ICPR 2006. 18th International Conference on*, volume 3, pages 850–855. IEEE, 2006.

[42] N. Papernot, P. McDaniel, S. Jha, M. Fredrikson, Z. B. Celik, and A. Swami. The limitations of deep learning in adversarial settings. In *2016 IEEE European Symposium on Security and Privacy (EuroS&P)*, pages 372–387. IEEE, 2016.

[43] N. Papernot, P. McDaniel, S. Jha, M. Fredrikson, Z. B. Celik, and A. Swami. The limitations of deep learning in adversarial settings. pages 372–387, 2016.

[44] N. Papernot, P. McDaniel, X. Wu, S. Jha, and A. Swami. Distillation as a defense to adversarial perturbations against deep neural networks. In *2016 IEEE Symposium on Security and Privacy (SP)*, pages 582–597. IEEE, 2016.

[45] S. Prokudin, D. Kappler, S. Nowozin, and P. Gehler. Learning to filter object detections. In *German Conference on Pattern Recognition*, pages 52–62. Springer, 2017.

[46] J. Redmon, S. Divvala, R. Girshick, and A. Farhadi. You only look once: Unified, real-time object detection. In *Proceedings of the IEEE conference on computer vision and pattern recognition*, pages 779–788, 2016.

[47] J. Redmon and A. Farhadi. Yolo9000: better, faster, stronger. *arXiv preprint arXiv:1612.08242*, 2016.

[48] J. Redmon and A. Farhadi. Yolov3: An incremental improvement. *arXiv preprint arXiv:1804.02767*, 2018.

[49] S. Ren, K. He, R. Girshick, and J. Sun. Faster r-cnn: Towards real-time object detection with region proposal networks. In *Advances in neural information processing systems*, pages 91–99, 2015.

[50] F. Schroff, D. Kalenichenko, and J. Philbin. Facenet: A unified embedding for face recognition and clustering. In *IEEE Conference on Computer Vision & Pattern Recognition*, 2015.

[51] M. J. Shafiee, B. Chywl, F. Li, and A. Wong. Fast yolo: A fast you only look once system for real-time embedded object detection in video. *arXiv preprint arXiv:1709.05943*, 2017.

[52] U. Shaham, Y. Yamada, and S. Negahban. Understanding adversarial training: Increasing local stability of supervised models through robust optimization. *Neurocomputing*, 2018.

[53] D. Song, K. Eykholt, I. Evtimov, E. Fernandes, B. Li, A. Rahmati, F. Tramer, A. Prakash, and T. Kohno. Physical adversarial examples for object detectors. In *12th {USENIX} Workshop on Offensive Technologies ({WOOT}) 18*, 2018.

[54] Y. Song, T. Kim, S. Nowozin, S. Ermon, and N. Kushman. Pixeldefend: Leveraging generative models to understand and defend against adversarial examples. *arXiv preprint arXiv:1710.10766*, 2017.

[55] C. Szegedy, W. Zaremba, I. Sutskever, J. Bruna, D. Erhan, I. Goodfellow, and R. Fergus. Intriguing properties of neural networks. *Computer Science*, 2013.

[56] F. Tramèr, A. Kurakin, N. Papernot, D. Boneh, and P. McDaniel. Ensemble adversarial training: Attacks and defenses. *arXiv preprint arXiv:1705.07204*, 2017.

[57] C. Xie, J. Wang, Z. Zhang, Y. Zhou, L. Xie, and A. Yuille. Adversarial examples for semantic segmentation and object detection. In *International Conference on Computer Vision*. IEEE, 2017.

[58] W. Xu, D. Evans, and Y. Qi. Feature squeezing: Detecting adversarial examples in deep neural networks. *arXiv preprint arXiv:1704.01155*, 2017.

[59] J. Zhang, M. Huang, X. Jin, and X. Li. A real-time chinese traffic sign detection algorithm based on modified yolov2. *Algorithms*, 10(4):127, 2017.

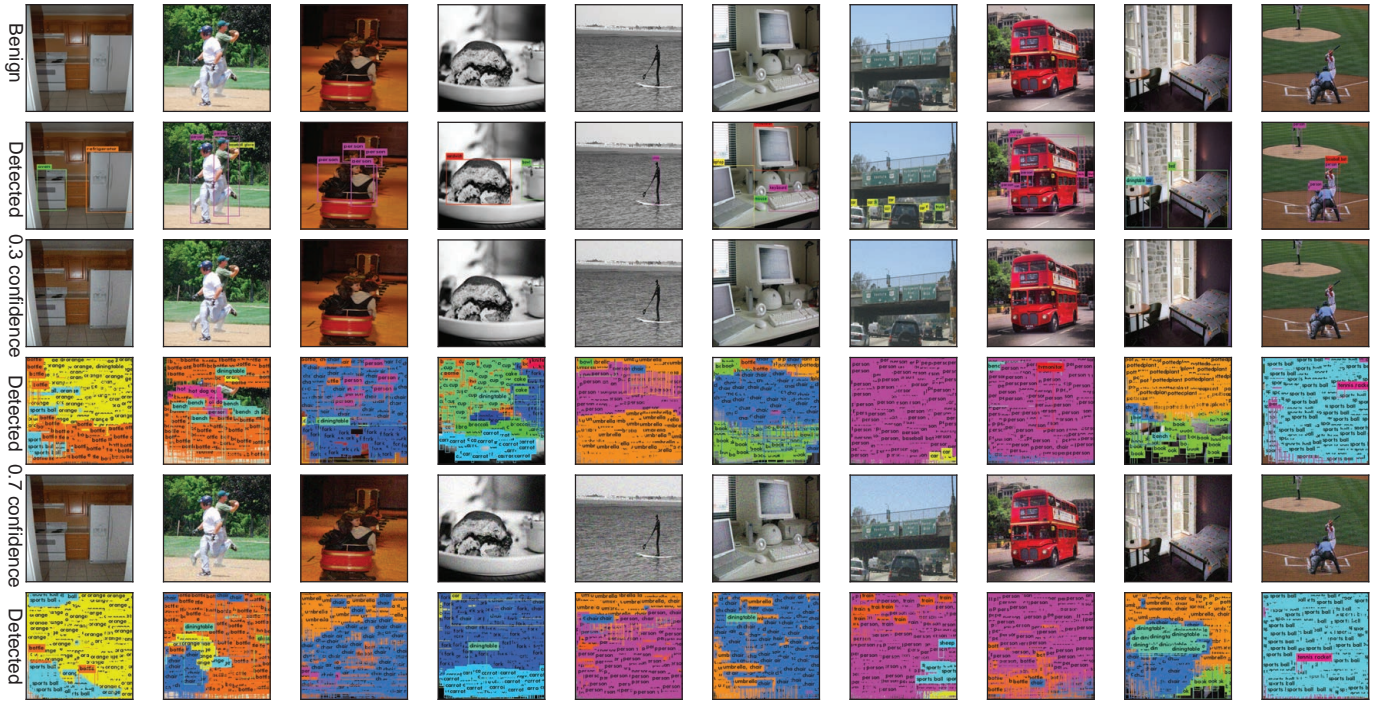


Fig. 18. Adversarial examples made by our L_0 attack. The first row contains the original images. The third row contains our low-confidence ($\gamma=0.3$) adversarial examples. The fifth row contains our high-confidence ($\gamma=0.7$) examples. The detection results from YOLO-v3 are in the rows below them. The confidence controls the density of the redundant detection boxes in the detection results.

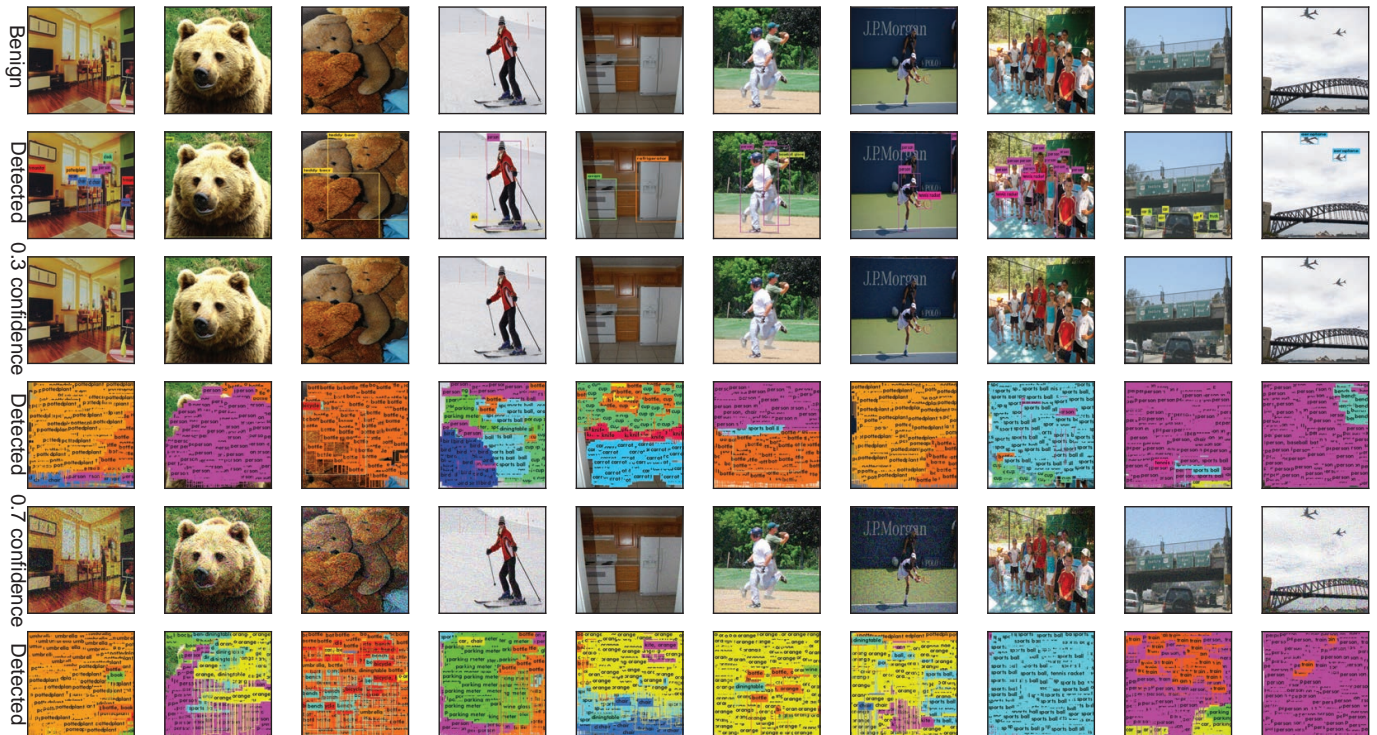


Fig. 19. Adversarial examples made by our L_2 attack. The first row contains the original images. The third row contains our low-confidence ($\gamma=0.3$) adversarial examples. The fifth row contains our high-confidence ($\gamma=0.7$) examples. The detection results from YOLO-v3 are in the rows below them. The confidence controls the density of the redundant detection boxes in the detection results.



Fig. 20. The detection results of Daedalus adversarial examples made by our L_2 attack towards RetinaNet-ResNet-50. The adversarial examples are crafted based on a confidence of 0.3.

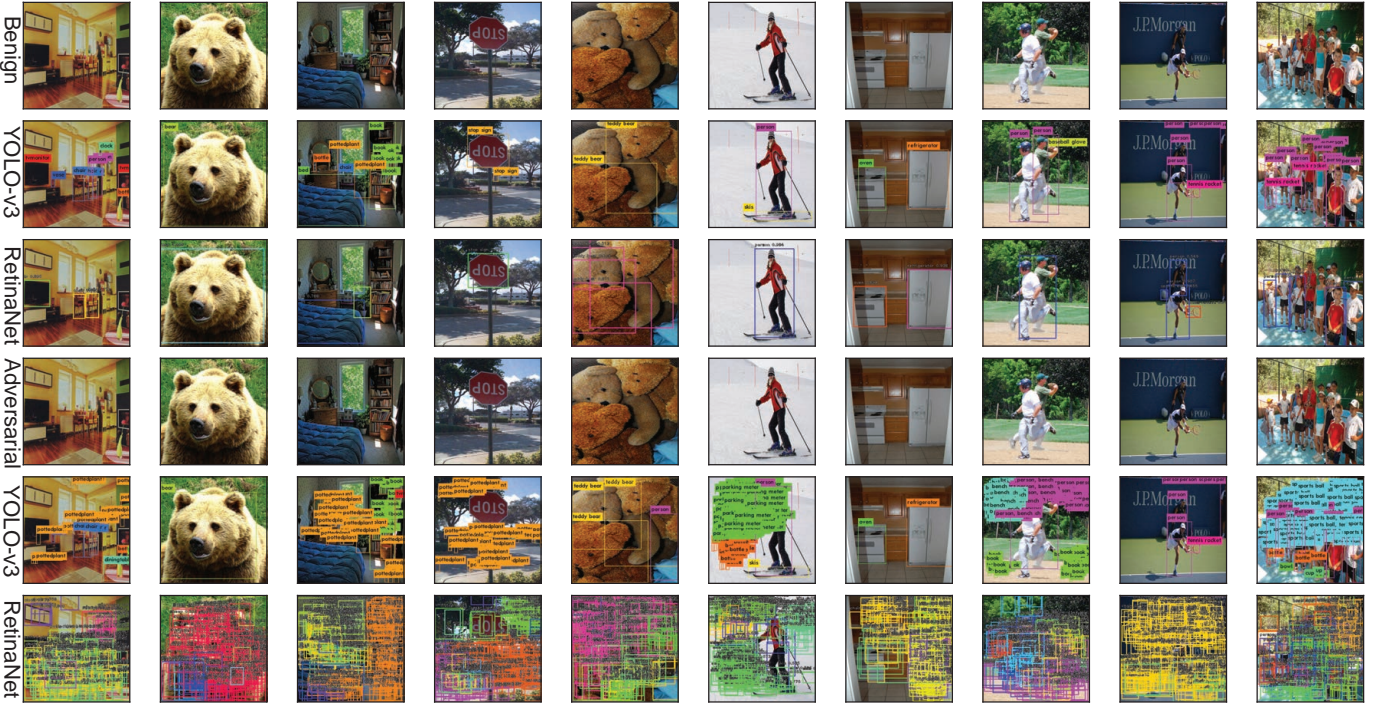


Fig. 21. The detection results of Daedalus adversarial examples made by our ensemble L_2 attack towards YOLO-v3 and RetinaNet. The adversarial examples are crafted based on a confidence of 0.3. The first row displays the benign examples. The second and the third rows are the detection results of the benign examples from YOLO-v3 and RetinaNet, respectively. The Daedalus examples are displayed in the fourth row. The detection results of the adversarial examples from YOLO-v3 and RetinaNet are in the fifth row and the last row, respectively.

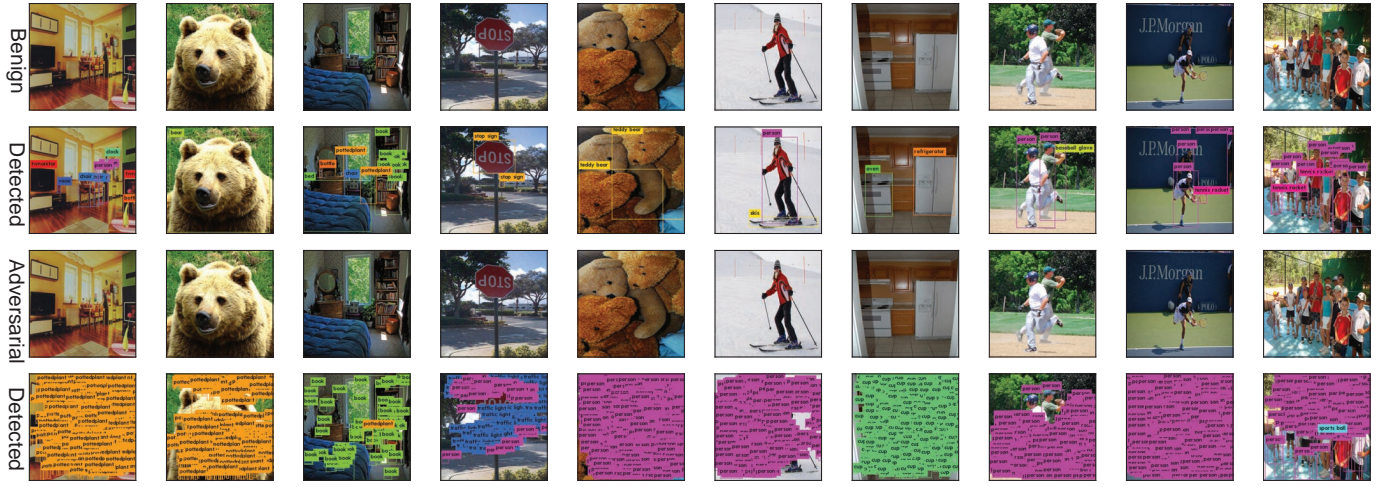


Fig. 22. Attacking the object category which has the most number of the detection boxes before NMS. The attacked model is YOLO-v3.



Fig. 23. Demonstration of attacking object in a specified category for YOLO-v3. We select 'person' to attack.



Fig. 24. Demonstration of attacking object in a specified category for YOLO-v3. We select 'car' to attack.